Geophysical Research Letters

RESEARCH LETTER
10.1029/2020GL090789

Impacts of Large-Scale Sahara Solar Farms on Global Climate and Vegetation Cover

Zhengyao Lu[1], Qiong Zhang[2], Paul A. Miller[1,3], Qiang Zhang[2], Ellen Berntell[2], and Benjamin Smith[1,4]

[1]Department of Physical Geography and Ecosystem Science, Lund University, Lund, Sweden, [2]Department of Physical Geography and Bolin Centre for Climate Research, Stockholm University, Stockholm, Sweden, [3]Centre for Environmental and Climate Research, Lund University, Lund, Sweden, [4]Hawkesbury Institute for the Environment, Western Sydney University, Penrith, NSW, Australia

Key Points:

- A set of state-of-the-art Earth-system model simulations are used to study the impacts of large-scale (20% coverage or more) Sahara solar farms
- These hypothetical solar farms increase local rainfall and vegetation cover through positive atmosphere–land(albedo)–vegetation feedbacks
- Conveyed by atmospheric teleconnections, the Sahara solar farms can induce remote responses in global climate and vegetation cover

Supporting Information:

- Supporting Information S1

Correspondence to:
Z. Lu,
zhengyao.lu@nateko.lu.se

Citation:
Lu, Z., Zhang, Q., Miller, P. A., Zhang, Q., Berntell, E., & Smith, B. (2021). Impacts of large-scale Sahara solar farms on global climate and vegetation cover. *Geophysical Research Letters*, *48*, e2020GL090789. https://doi.org/10.1029/2020GL090789

Received 11 SEP 2020
Accepted 7 DEC 2020

Abstract Large-scale photovoltaic solar farms envisioned over the Sahara desert can meet the world's energy demand while increasing regional rainfall and vegetation cover. However, adverse remote effects resulting from atmospheric teleconnections could offset such regional benefits. We use state-of-the-art Earth-system model simulations to evaluate the global impacts of Sahara solar farms. Our results indicate a redistribution of precipitation causing Amazon droughts and forest degradation, and global surface temperature rise and sea-ice loss, particularly over the Arctic due to increased polarward heat transport, and northward expansion of deciduous forests in the Northern Hemisphere. We also identify reduced El Niño-Southern Oscillation and Atlantic Niño variability and enhanced tropical cyclone activity. Comparison to proxy inferences for a wetter and greener Sahara ~6,000 years ago appears to substantiate these results. Understanding these responses within the Earth system provides insights into the site selection concerning any massive deployment of solar energy in the world's deserts.

Plain Language Summary Solar energy can contribute to the attainment of global climate mitigation goals by reducing reliance on fossil fuel energy. It is proposed that massive solar farms in the Sahara desert (e.g., 20% coverage) can produce energy enough for the world's consumption, and at the same time more rainfall and the recovery of vegetation in the desert. However, by employing an advanced Earth-system model (coupled atmosphere, ocean, sea-ice, terrestrial ecosystem), we show the unintended remote effects of Sahara solar farms on global climate and vegetation cover through shifted atmospheric circulation. These effects include global temperature rise, particularly over the Arctic; the redistribution of precipitation (most notably droughts and forest degradation in the Amazon) and northward shift of the Intertropical Convergence Zone; the northward expansion of deciduous forests in the Northern Hemisphere; and the weakened El Niño-Southern Oscillation and Atlantic Niño variability and enhanced tropical cyclone activity. All these remote effects are in line with the global impacts of the Sahara land-cover transition ~6,000 years ago when Sahara desert was wetter and greener. The improved understanding of the forcing mechanisms of massive Sahara solar farms can be helpful for the future site selection of large-scale desert solar energy facilities.

1. Introduction

Despite the rapid depletion of global reserves (Shafiee & Topal, 2009) and harmful effects on global climate (IPCC, 2018), fossil fuel burning continues to dominate energy systems worldwide (Johansson et al., 2012). Solar farms offer an attractive solution for the transition to clean and sustainable energy use: solar power is the most abundant available renewable energy source (Johansson et al., 2012; Sieminski, 2013) and helps to mitigate climate change through reduced emissions (Creutzig et al., 2017; Kannan & Vakeesan, 2016). Harvesting the globally available solar energy (or even just that over the Sahara) could theoretically meet all humanity's energy needs today (Hu et al., 2016; Li et al., 2018). Large-scale deployment of solar facilities over the world's deserts has been advanced as a feasible option (Komoto et al., 2015).

The climate and environmental impacts of solar farms have drawn increasing attention due to the rapid development of solar energy. Indeed, both on-site (e.g., Barron-Gafford et al., 2016; Grodsky & Hernandez, 2020; Y. Liu et al., 2019) and satellite (e.g., Zhang & Xu, 2020) observations have shown complex and

location-dependent changes to microclimates and shifts in local ecosystems after the construction of desert solar farms across the world. Competing responses in surface temperature warming and cooling, and ecosystem recovery and degradation, were reported in prior work. These effects remain highly uncertain and motivate modeling studies to assess the potential regional and global impacts of the proposed large-scale application of solar energy in the desert based on a range of future energy use scenarios (Hu et al., 2016). The primary mechanism for local impacts can be largely simplified to a land–atmosphere feedback due to the albedo change in the desert, which is also the mechanism through which overgrazing has been implicated to, at least partly, cause Sahel droughts (Charney, 1975). Similar land use/land-cover changes have been found to trigger this feedback and induce local climate and ecosystem responses, particularly over arid/semiarid regions (Huang et al., 2017). Interestingly, a recent modeling study (Li et al., 2018)—the first to link this land–atmosphere feedback to solar farms—reported that large-scale solar farms in the Sahara desert would increase local rainfall and vegetation, benefitting both the regional environment and sustainable development while generating electricity in excess of current global consumption. In simulations with a global atmosphere model with a dynamic land surface, the darker land surface (lower albedo of photovoltaic [PV] panels) compared to the desert surfaces they mask induces higher surface air temperatures and convergent flow. This, in turn, leads to more rainfall and promotes vegetation growth. The expansion of vegetation cover further lowers the surface albedo, amplifying the initial warmer and wetter conditions through this positive feedback. However, these local responses would also be expected to induce remote impacts through atmospheric teleconnections and ocean dynamics. These effects, which could significantly alter the assessment of the mitigation potential of solar farms, could not be fully captured by the model employed in Li et al. (2018), due to the assumption of unchanging ocean temperatures and heat transport.

2. Materials and Methods

2.1. The Earth-System Model EC-Earth

We employ a fully coupled Earth-system model (ESM), EC-Earth to study the global climate and environmental responses to large-scale solar farms in the Sahara. EC-Earth (version 3.3.1) is a European community ESM which integrates several component models (atmosphere, ocean, sea-ice, and dynamic vegetation) and thus is capable of simulating complex interactions between the atmosphere, the ocean, and the land biosphere. In addition to incorporating a full set of interacting components affecting large-scale climate, EC-Earth employs a relatively high atmospheric spatial resolution that can more accurately represent synoptic precipitation (Raj et al., 2019) and boundary layer conditions (e.g., better resolved topography) (Zheng & Eltahir, 1998), important for capturing key dynamic features of the Sahara regional climate system such as the Western African Monsoon (WAM) strength (Hourdin et al., 2010; Sylla et al., 2010; Xue et al., 2010). Past studies (Hazeleger et al., 2010, 2012; Kageyama et al., 2017) provide an overview of the general performance of an earlier version of this model. In particular, the model demonstrates skill in emulating a number of key physical processes relevant to this study, such as the atmospheric general circulation and monsoon system (Berntell et al., 2018; Pausata et al., 2016) and the tropical climate variability and atmospheric teleconnections (Pausata et al., 2017a). A recent study shows that simulated 100-year trends and interdecadal variability of EC-Earth (EC-Earth3-Veg configuration, also used in this study) fall within the range of the CMIP6 (the latest ESM Intercomparison project) piControl ensemble (Parsons et al., 2020).

EC-Earth is part of a new generation of global ESMs that incorporates a second-generation dynamic vegetation–ecosystem scheme (the LPJ-GUESS vegetation–ecosystem model) based on an individual-based and patch-based representation of land ecosystem structure and dynamics (Smith et al., 2001, 2014). It takes into account vegetation structure, competition, and disturbances which are key to accurately modeling responses of dry land and mixed forest ecosystems (Smith et al., 2014; Whitley et al., 2017). This functionality has been demonstrated to be critical for capturing tree mortality and recovery following drought in savannahs and forest ecosystems (Haverd et al., 2013; Purves & Pacala, 2008; Wolf et al., 2011). Associated interactions with climate are key to characterizing the impacts and feedbacks of land use and land-cover changes in regions sensitive to altered albedo, such as the Sahara desert. The model shows improved performance in arid land like North Africa, for example, for the precipitation–grass cover relationship (Lu et al., 2018).

2.2. Solar Farm Simulations

We conduct three baseline simulations (CTRL, S20, and S50) using the fully coupled EC-Earth model 3.3.1 with active atmosphere, ocean, sea-ice, and dynamic vegetation components. The horizontal resolution of atmosphere/land/vegetation is T159 (∼1.125°), with 62 vertical levels in the atmosphere, while the ocean/sea-ice model has a horizontal resolution of ∼1° and 46 vertical levels. Each simulation is initialized from a state of 1990 climate and vegetation cover (representing a present-day state for this model which is constrained by observation) and runs for 150 years during spin-up. The model reaches a quasi-equilibrium climate (indicated by the stable global mean surface air temperature and Sea Surface Temperature [SST], figure not shown) after spin-up, and we use the next 60 years of model output for analysis. We fix the greenhouse gas levels, aerosol forcing, and other land use and land-cover properties (cropland, pasture, and managed forest) at their 1990 values.

The S20 and S50 ("solar panels") represent the "Sahara solar farm" scenarios in which 20% and 50% of all the grid points in the North African region (15–30°N, 20°W–45°E; Figure 3, black circles; Figure S1) are prescribed reduced bare soil albedo. The installment of PV panels decreases surface albedo from the highly reflective desert soils (Figure S1). The albedo of the entire prescribed grid point approximates the *effective albedo* (0.235) of PV solar panels (Li et al., 2018) (Text S1). The *effective albedo* of PV panels takes account of the lateral export of electric energy captured by the panels outside the deployment region (Text S1). For simplicity, vegetation is allowed to grow in solar panel grid cells and change their cover fraction, but the influence of this unrealistic assumption is expected to be limited in terms of albedo effects (Text S1). Note that this method (lowering surface albedo) has been commonly used in climate models and ESMs to study large-scale PV solar farm impacts (e.g., Hu et al., 2016; Li et al., 2018). The S20 and S50 scenario simulations are compared with a 1990 control simulation (CTRL).

The low-end scenario S20 is expected to be able to meet the global demand after various efficiency losses, and its justification in terms of electricity production can be found in Text S2. S20 is also ideal for an inter-model comparison with Li et al. (2018). The high-end scenario S50 is a more theoretical scenario to focus on the forcing mechanisms from larger signals in land use changes (Text S2). Another regional consumption scenario (S05) in which solar panels cover 5% of North Africa and supply the energy needs of Europe, Africa, and the Middle East (∼24.6% of the world's consumption; BP, 2019) is also considered, the results of which are discussed in Text S3.

We also conduct two additional simulations driven by the mean SST seasonal cycle calculated from the reanalysis data for the period 1960–1989 (Hurrell et al., 2008) ($CTRL_{SST}$ and $S20_{SST}$). This ensures that in these simulations only changes to the atmosphere and vegetation are simulated and allow us to disentangle the effects of interactive ocean dynamics. In $S20_{SST}$, we use the same configuration of solar panels as in S20. These fixed SST simulations are similar to those studied in Li et al. (2018). By comparing the response of climate and vegetation in $S20_{SST}$ and $CTRL_{SST}$ (a 30-year interval of output) to that in the fully coupled simulations S20 and CTRL, we can assess the role of ocean dynamics (and resulting ocean–atmosphere interactions) and land-induced changes in atmospheric dynamics in propagating the local influences of Sahara solar farms to a global scale.

3. Results

3.1. Local Response to the Sahara Solar Farms

The EC-Earth solar farm simulations depict prominent warming anomalies over the Sahara (Figures 1a–c). The local mean surface air temperature is increased by ∼1.5°C in S20 and is further increased by ∼1°C in S50. This corresponds to ∼1°C of warming per 4.4% reduction of the surface albedo (Figure S4, taking vegetation cover into account), consistent with a previous study (Laguë et al. 2019). To the south of the local warming signal is a slight cooling, where latent heat cooling (because of more precipitation) and enhanced vegetation evapotranspiration dominates, especially during boreal summer (Figure S3a-c). The precipitation response (Figures 1d–f) is closely associated with temperature anomalies. The increased annual mean precipitation is driven by surface heating and moisture convergence (Figure S5), mainly in summer (Figure S3d–f). The precipitation increase averaged over the Sahara desert is 0.1 and 0.4 mm/day in S20 and S50,

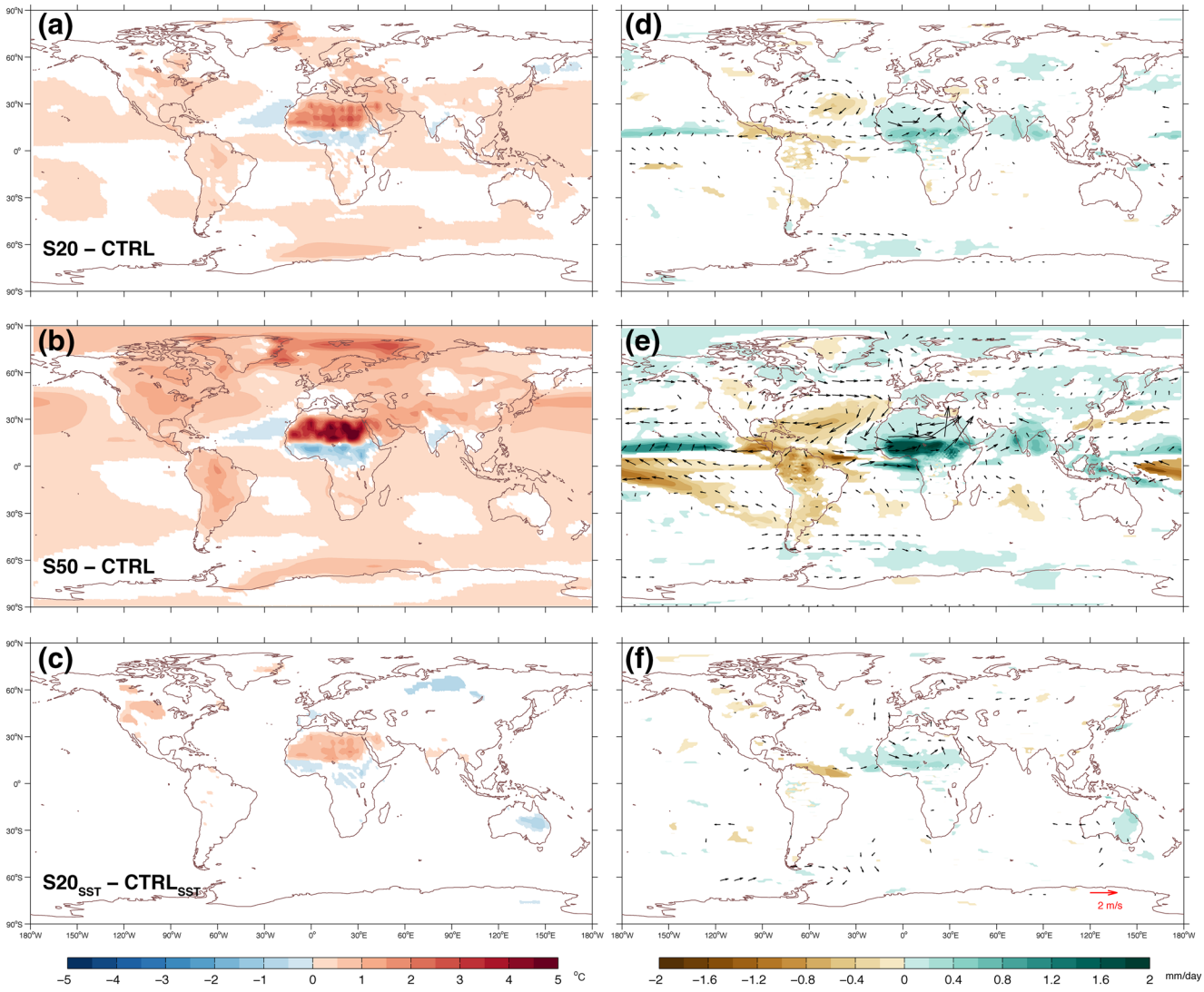

Figure 1. Mean climate response. Modeled annual mean (a–c) surface air temperature response, and (d–f) precipitation and 925 hPa wind response. From top to bottom, the results are for S20−CTRL, S50−CTRL, and $S20_{SST}$−$CTRL_{SST}$. All anomalies shown exceed 95% significance level based on two-sample *t* test.

respectively, with larger increases at the southern edge of the area (Figures 1d–f; Figure S4). Circulation shifts are a key to these rainfall changes, mainly driven by an enhanced WAM (Figure S3d–f). The spatial pattern and magnitude of the local temperature and precipitation anomalies of S20 and $S20_{SST}$ are consistent with Li et al. (2018).

More rainfall over North Africa induced by large-scale solar farms leads to vegetation expansion (Figures 2a–2c). In S20, the vegetation extent shifts northward only slightly, whereas in S50 about half of the Sahara becomes colonized by savannah and grassland. By comparing vegetation coverage (Figures 2d–2g), we identify that the Sahara vegetation change mainly consists of expansion of tall grass with scattered high vegetation including closed rainforest as far north as ~30°N in the S50 scenario. In the desert, vegetation growth enabled by rainfall enhancement further reduces albedo, increases evapotranspiration, and decreases sensible heat flux; this reinforces the initial precipitation increase and leads to a larger vegetation response (Li et al., 2018). As a result, the simulated vegetation expansion, which in the Sahara mostly consists of grass replacing bare ground, induces positive land (vegetation)–atmosphere feedbacks (Lu et al., 2018; Pausata et al., 2016). This local positive albedo–precipitation–vegetation feedback is also known as the classic Charney mechanism (Charney, 1975).

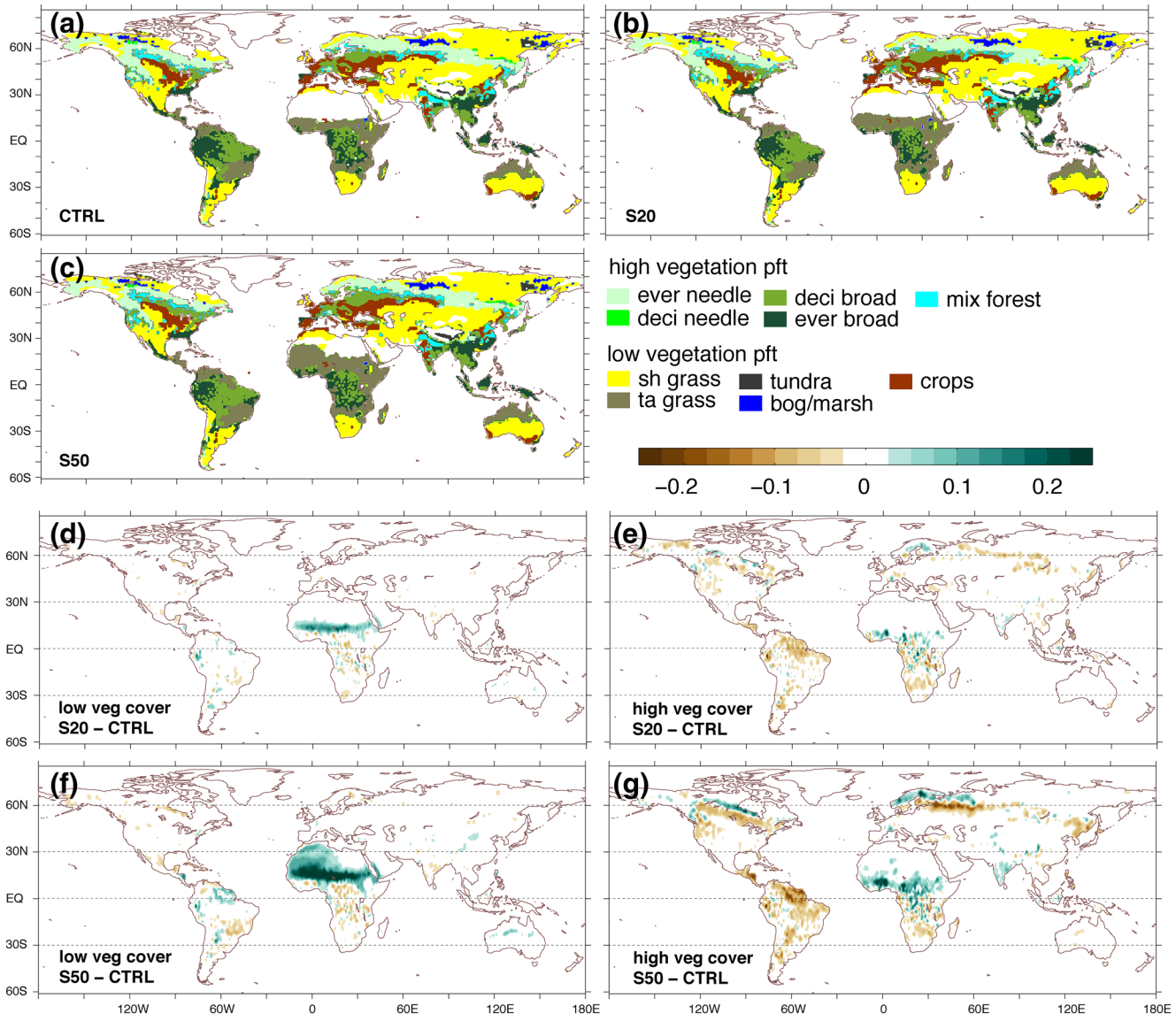

Figure 2. Vegetation response. Modeled vegetation pattern of (a) CTRL, (b) S20, and (c) S50. The simulated plant functional type (PFT) is shown where the vegetation cover is larger than 15%. Modeled annual mean vegetation cover (fraction) differences for (d, f) low vegetation and (e, g) high vegetation.

3.2. Remote Response to the Sahara Solar Farms

Our simulations reveal that the climate response to a massive deployment of solar farms is not limited to the local scale but is characterized by extensive teleconnections. Both the S20 and S50 scenarios lead to a pronounced signal of surface warming across the globe (Figure 1a and 1b), and in the case of S50 it can be seen more clearly that the warming is stronger in the Northern Hemisphere high latitudes. In contrast, the temperature response outside the North African region is largely suppressed when SST is prescribed in the simulations (Figure 1c). The mechanism behind the remote response is as follows: the local response of warming in North Africa leads to a stronger meridional temperature gradient between the subtropics and high latitudes, thus intensifying the mid-latitude to high-latitude eddy activity and oceanic Atlantic meridional overturning circulation (Figure S6a). This also results in larger northward atmospheric and oceanic heat transport (Figure S6b,c) (Muschitiello et al., 2015). The Arctic climate shift in S50 also indicates the presence of a persistent positive Arctic Oscillation pattern, with lower sea level pressure over the Arctic (Figure S7, shading), stronger winds circulating around the North Pole (Figure S7, vectors), and more cold air confined to the polar regions. However, this Arctic amplification is not very clear in S20.

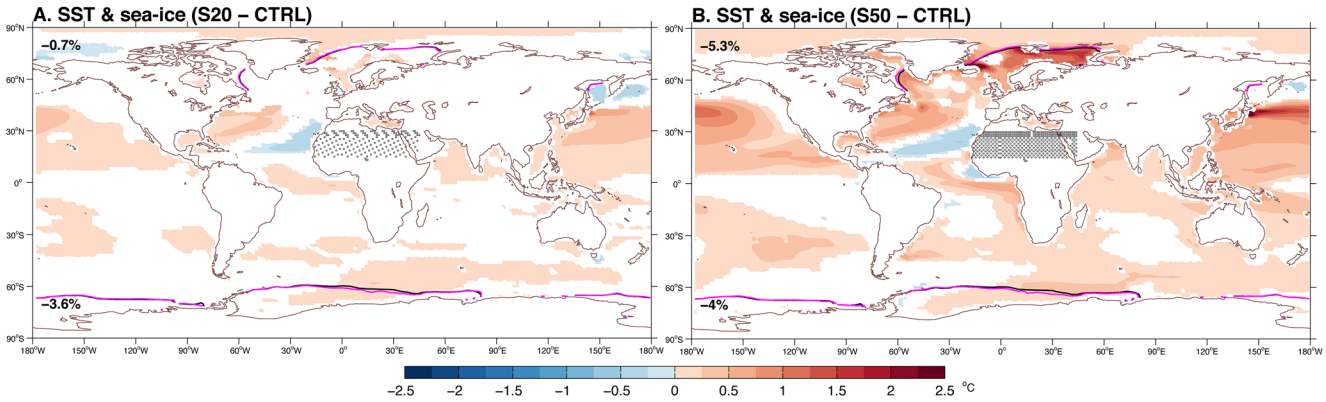

Figure 3. Ocean mean state response. Modeled annual mean SST response (shading color) and sea-ice extent (>50% sea-ice concentration) in CTRL (black curve) and solar farm simulations (purple curves) for (a) S20−CTRL and (b) S50−CTRL. The hemispheric sea-ice extent changes are also shown in the corner of the map. Black dots depict the locations of solar panels for S20 and S50 ("checkerboard"). All anomalies shown exceed 95% significance level based on two-sample *t* test.

The most striking feature of the mean SST response is the warming of the Arctic Ocean, North Pacific, and North Atlantic (Figure 3a and 3b, shading), while the warming effect on the Southern Ocean is smaller. This North-South asymmetric warming is more robust in S50, reaching +2°C in the oceans in the North Hemisphere. Accompanied by the warming anomalies, the Arctic and Antarctica sea-ice decline is noticeable in the solar farm simulations (Figure 3a and 3b, black and purple contours, numbers) but generally weaker in S20. The SST cools slightly in the equatorial Atlantic (likely due to increased wind-driven coastal upwelling off Northwest Africa) and causes a larger east-west temperature gradient, related to the intensification of the WAM (Pausata et al., 2016).

Solar farms induce a northward shift in the Intertropical Convergence Zone (ITCZ) in the tropical Pacific (as seen from the precipitation anomalies; Figure 1d and 1e), driven by warming in the Northern Hemisphere and the enhanced meridional heat transport (Figure 1a and 1b; Figure S6) (Chiang & Friedman, 2012). The precipitation response includes a significant reduction (by ∼−10% in S20 and ∼−30% in S50) over vast regions of Central America, northern South America, and the tropical western Atlantic, in about half of a magnitude of precipitation increase seen in the Sahel and Sahara (Figure 1d and 1e). Moisture supply to those regions declines (Figure S5a,b, vectors), perturbed by the large-scale atmospheric circulation changes (Durán-Quesada et al., 2017). The moisture source in the Atlantic instead transports more to the Sahel and that in the Pacific transports more to the northward shifted Pacific ITCZ. The reduction in moisture flow and precipitation over the Amazon can be further exacerbated by the remote effects from vegetation expansion over Africa (Kooperman et al., 2018). By examining the large-scale remote responses induced by Sahara solar farms in $S20_{SST}$, we find that the precipitation and wind anomalies seen in S20 are significantly dampened when the ocean response to local changes and associated ocean–atmosphere interactions are limited (Figure 1f; Figure S3f).

The solar farm simulations show a consistent decline in El Niño-Southern Oscillation (ENSO) variability (Text S4), from −3% in S20% to −17% in S50 (averaged over Niño 3.4 box) (Figures 4a–4c). The Atlantic Niño variability is also reduced in S20 and considerably weakened in S50. The early onset of the WAM (not shown) and the northward shift of ITCZ in late spring and summer decrease the equatorial western Atlantic surface wind variability, as the maximum wind variance moves away from the equator. This in turn weakens the equatorial eastern Atlantic SST variability (which usually peaks a few months later) (Pausata et al., 2017a). The Atlantic Niño response further increases the strength of the Walker circulation (Figure S8a,b) and drives the wind anomalies over the equatorial Pacific westwards during summer (Figure S3d,e). This leads to increased mean westward ocean currents and a deepened thermocline in the equatorial Pacific (FigureS8c). The former can dampen the eastward-propagating warm surface anomalies that characterize extreme El Niño events (Cai et al., 2015), and the latter can weaken the Bjerknes positive feedbacks (Liu et al., 2014) by reducing ocean vertical stratification which is crucial for ENSO development (Ding et al., 2012).

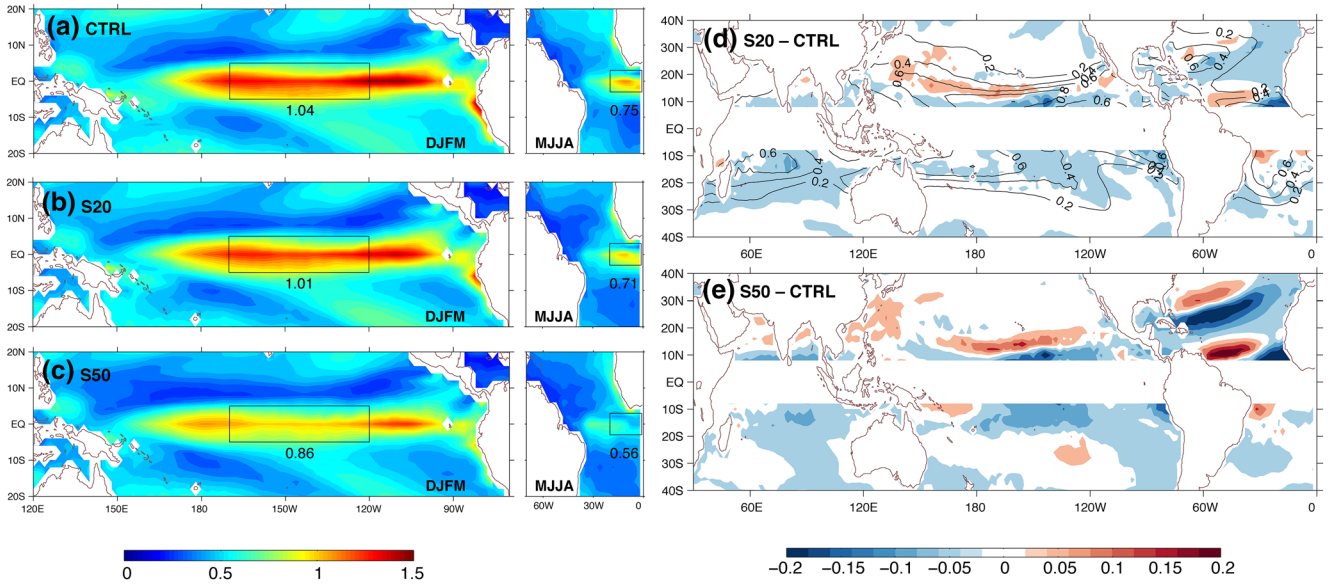

Figure 4. El Niño, Atlantic Niño, and tropical cyclone response. (a–c) Modeled SST interannual variability for the Pacific basin (DJFM) and Atlantic basin (MJJA) (Text S4). Black boxes are Niño3.4 and Atlantic3 regions with the region averaged value shown below. (d, e) Modeled CGI index (Text S5) change (shading color) with mean CGI index of CTRL shown in (d) as black contour. The CGI is set to zero between 5°S and 5°N due to zero Coriolis vorticity at the equator. CGI, Cyclone Genesis Index.

Solar farms tend to promote more favorable conditions for tropical cyclone development. By examining a Cyclone Genesis Index (CGI) (Text S5) (Bruyère et al., 2012), we estimate how the climate state, in particular the kinematic (wind shear) and thermodynamic (potential intensity) factors, affects the tropical cyclogenesis in our simulations. The changes to CGI in S20 and S50 indicate that tropical cyclone activity is likely to be amplified in the Northern Hemisphere in these scenarios, especially off the East Asian coast and North America (Figure 4d and 4e). The North Atlantic tropical cyclone formation area (Figure 4d, contour) is shifted to the western North Atlantic margin, leading to the dipole pattern in the CGI anomalies. This potential intensification of tropical cyclone genesis in the coastal regions is mainly attributed to increased potential intensity and weakened vertical wind shear in these regions (Figure S9), linked to the northward expansion of the ITCZ (Pausata et al., 2017a; Van Hengstum et al., 2016).

4. Discussion and Conclusion

Our ESM simulation results support the hypothesis that theoretical large-scale solar farms in the Sahara desert can bring more rainfall and vegetation to this region, and at the same time meet the energy demand of the global population (Text S2) (Li et al., 2018), currently at 18.4 TW and steadily increasing (BP, 2019). However, the remote effects of these solar farms on global climate and ecosystems as conveyed through atmospheric teleconnections and reinforced by ocean dynamics appear to be robust. The analogous local rainfall increase and global climate changes during the "Green Sahara" wet period ~6,000 years ago (Claussen et al., 2017)—supported by various proxy data and modeling studies (Text S6)—rationalize our model sensitivity to landscape changes (albedo) in North Africa. These results suggest that careful spatial planning and improved solar panel efficiency will be needed to minimize the unintended consequences of massive desert solar farms in North Africa.

It should be noted that the potential risks in remote regions associated with the deployment of Sahara solar farms can be scale dependent and model dependent. In our model, for instance, if the solar farms do not cover a large enough fraction of the Sahara desert (20% coverage or more), then the responses are quite muted (e.g., the S05 scenario, Text S3). A more comprehensive assessment of such risks would also require a systematic study using more ESM simulations with different model sensitivities to land use changes. Moreover, in future studies, the global impacts of large-scale solar farms should be evaluated alongside the

effect of reduced CO_2 emissions from fossil fuels brought on by the deployment of such solar farms. In fact, the warming from anthropogenic emissions of CO_2 from fossil fuels would likely exceed the global surface temperature rise of 0.16 and 0.39°C caused by solar farms in S20 and S50.

The implementation of solar panels as decreased bare soil albedo in our simulations can be seen as oversimplified, and some unique solar panel properties may need to be considered with their effects quantified in future studies. The interface between air and soil is different from that between air and impervious solar panels. In the solar farm simulations, the additional absorbed solar radiation is dissipated through the surface energy balance (the model scheme is described in Verhoef & Vidale, 2012) and manifests as surface flux and temperature changes through thermal and water-holding properties of soil, compared to those through albedo and heat capacity of solar panels. Furthermore, the desert solar panels are usually placed above the ground, and they may also lead to changes in wind speed, turbulence, and mixing in the near-surface boundary layer (Armstrong et al., 2014). Vegetation grows over the soil (prescribed solar panels in the simulations) which is not likely in a well-managed solar farm, while it can overestimate the increase in evapotranspiration.

There are other essential aspects of the global response to desert solar farms that are currently missing in our simulations but can be assumed as important side effects. They partly justify the design of more stylized scenario S50 so that we are able to fully capture potential global impacts compared to S20 that is more closely related to the world's projected energy use. For example, the vegetation recovery over the desert zone can cause a drop in dust loadings (also reducing albedo) which can directly contribute to the local atmosphere–land(albedo)–vegetation feedback and cause additional local and remote atmosphere, ocean, and land surface responses (Pausata et al., 2016). The reduced dust emission from North Africa can further affect the fertilization of the Amazon forest (Yu et al., 2015) and the Atlantic Ocean phytoplankton (Conway & John, 2014) through long-range transport, triggering amplified ecosystem shifts. All these potential coupled responses underscore the importance of a holistic, Earth-system analysis when examining the benefits and risks of the expansive establishment of solar farms in the world's deserts.

Data Availability Statement

All data analyzed in the paper for the main figures are accessible in the Harvard Dataverse repository at https://doi.org/10.7910/DVN/TEZW3N.

Acknowledgments
The authors greatly appreciate constructive comments from two anonymous reviewers. This study is a contribution to the strategic research area MERGE and Swedish Research Council (VR) funded project "Simulating green Sahara with Earth System Model" (2017-04232). Z. Lu received funding from FORMAS mobility (Grant no. 2020-02267). The authors thank Drs Klaus Wyser, Philippe Le Sager, Emanuel Dutra, and Jost von Hardenberg for their useful comments on the experiment set-up. The EC-Earth simulations were performed on resources provided by the Swedish National Infrastructure for Computing (SNIC) at Linköping University.

References

Armstrong, A., Waldron, S., Whitaker, J., & Ostle, N. J. (2014). Wind farm and solar park effects on plant–soil carbon cycling: Uncertain impacts of changes in ground-level microclimate. *Global Change Biology*, *20*(6), 1699–1706.

Barron-Gafford, G. A., Minor, R. L., Allen, N. A., Cronin, A. D., Brooks, A. E., & Pavao-Zuckerman, M. A. (2016). The photovoltaic heat island effect: Larger solar power plants increase local temperatures. *Scientific Reports*, *6*, 35070.

Berntell, E., Zhang, Q., Chafik, L., & Körnich, H. (2018). Representation of multidecadal Sahel rainfall variability in 20th century reanalyses. *Scientific Reports*, *8*(1), 10937.

BP. (2019). *Statistical review of world energy*. https://www.bp.com/en/global/corporate/energy-economics/statistical-review-of-world-energy.html

Bruyère, C. L., Holland, G. J., & Towler, E. (2012). Investigating the use of a genesis potential index for tropical cyclones in the North Atlantic basin. *Journal of Climate*, *25*(24), 8611–8626.

Cai, W., Santoso, A., Wang, G., Yeh, S.-W., An, S.-I., Cobb, K. M., et al. (2015). ENSO and greenhouse warming. *Nature Climate Change*, *5*(9), 849.

Charney, J. G. (1975). Dynamics of deserts and drought in the Sahel. *Quarterly Journal of the Royal Meteorological Society*, *101*(428), 193–202.

Chiang, J. C. H., & Friedman, A. R. (2012). Extratropical cooling, interhemispheric thermal gradients, and tropical climate change. *Annual Review of Earth and Planetary Sciences*, *40*, 383–412.

Claussen, M., Dallmeyer, A., & Bader, J. (2017). Theory and modeling of the African humid period and the green Sahara. In Oxford Research Encyclopedia of Climate Science (49 pp.). Oxford University Press. https://doi.org/10.1093/acrefore/9780190228620.013.532

Conway, T. M., & John, S. G. (2014). Quantification of dissolved iron sources to the north Atlantic Ocean. *Nature*, *511*(7508), 212.

Creutzig, F., Agoston, P., Goldschmidt, J. C., Luderer, G., Nemet, G., & Pietzcker, R. C. (2017). The underestimated potential of solar energy to mitigate climate change. *Nature Energy*, *2*(9), 17140.

Ding, H., Keenlyside, N. S., & Latif, M. (2012). Impact of the equatorial Atlantic on the El Niño southern oscillation. *Climate Dynamics*, *38*(9–10), 1965–1972.

Durán-Quesada, A. M., Gimeno, L., & Amador, J. (2017). Role of moisture transport for Central American precipitation. *Earth System Dynamics*, *8*(1), 147–161.

Grodsky, S. M., & Hernandez, R. R. (2020). Reduced ecosystem services of desert plants from ground-mounted solar energy development. *Nature Sustainability*, *3*, 1036–1043. https://doi.org/10.1038/s41893-020-0574-x

Haverd, V., Smith, B., Cook, G. D., Briggs, P. R., Nieradzik, L., Roxburgh, S. H., et al. (2013). A stand-alone tree demography and landscape structure module for Earth system models. *Geophysical Research Letters*, *40*, 5234–5239. https://doi.org/10.1002/grl.50972

Hazeleger, W., Severijns, C., Semmler, T., Ştefănescu, S., Yang, S., Wang, X., et al. (2010). EC-earth: A seamless earth-system prediction approach in action. *Bulletin of the American Meteorological Society*, *91*(10), 1357–1364.

Hazeleger, W., Wang, X., Severijns, C., Ştefănescu, S., Bintanja, R., Sterl, A., et al. (2012). EC-earth V2. 2: Description and validation of a new seamless earth system prediction model. *Climate Dynamics*, *39*(11), 2611–2629.

Hourdin, F., Musat, I., Guichard, F. S., Ruti, P. M., Favot, F., Filiberti, M.-A., et al. (2010). AMMA-model intercomparison project. *Bulletin of the American Meteorological Society*, *91*(1), 95–104.

Hu, A., Levis, S., Meehl, G. A., Han, W., Washington, W. M., Oleson, K. W., et al. (2016). Impact of solar panels on global climate. *Nature Climate Change*, *6*(3), 290.

Huang, J., Li, Y., Fu, C., Chen, F., Fu, Q., Dai, A., et al. (2017). Dryland climate change: Recent progress and challenges. *Reviews of Geophysics*, *55*, 719–778. https://doi.org/10.1002/2016RG000550

Hurrell, J. W., Hack, J. J., Shea, D., Caron, J. M., & Rosinski, J. (2008). A new sea surface temperature and sea ice boundary dataset for the Community Atmosphere Model. *Journal of Climate*, *21*(19), 5145–5153.

Johansson, T. B., Patwardhan, A. P., Nakićenović, N., & Gomez-Echeverri, L. (2012). *Global energy assessment: Toward a sustainable future*, Cambridge, UK: Cambridge University Press.

Kageyama, M., Albani, S., Braconnot, P., Harrison, S. P., Hopcroft, P. O., Ivanovic, R. F., et al. (2017). The PMIP4 contribution to CMIP6—Part 4: Scientific objectives and experimental design of the PMIP4-CMIP6 Last Glacial Maximum experiments and PMIP4 sensitivity experiments. *Geoscientific Model Development*, *10*(11), 4035–4055.

Kannan, N., & Vakeesan, D. (2016). Solar energy for future world:-A review. *Renewable and Sustainable Energy Reviews*, *62*, 1092–1105.

Komoto, K., Ehara, T., Xu, H., Lv, F., Wang, S., Sinha, P., et al. (2015). *Energy from the desert: Very large scale PV power plants for shifting to renewable energy future*, Paris, France: International Energy Agency (IEA-PVPS Task 8). https://iea-pvps.org/wp-content/uploads/2020/01/Energy_from_the_desert_Ed-5_2015_lr.pdf

Kooperman, G. J., Chen, Y., Hoffman, F. M., Koven, C. D., Lindsay, K., Pritchard, M. S., et al. (2018). Forest response to rising CO_2 drives zonally asymmetric rainfall change over tropical land. *Nature Climate Change*, *8*(5), 434–440.

Laguë, M. M., Bonan, G. B., & Swann, A. L. (2019). Separating the impact of individual land surface properties on the terrestrial surface energy budget in both the coupled and uncoupled land–atmosphere system. *Journal of Climate*, *32*(18), 5725–5744.

Liu, Z., Lu, Z., Wen, X., Otto-Bliesner, B. L., Timmermann, A., & Cobb, K. M. (2014). Evolution and forcing mechanisms of El Niño over the past 21,000 years. *Nature*, *515*(7528), 550.

Liu, Y., Zhang, R. Q., Huang, Z., Cheng, Z., López-Vicente, M., Ma, X. R., &(2019). Solar photovoltaic panels significantly promote vegetation recovery by modifying the soil surface microhabitats in an arid sandy ecosystem. *Land Degradation & Development*, *30*(18), 2177–2186.

Lu, Z., Miller, P. A., Zhang, Q., Zhang, Q., Wårlind, D., Nieradzik, L., et al. (2018). Dynamic vegetation simulations of the mid-Holocene green Sahara. *Geophysical Research Letters*, *45*, 8294–8303. https://doi.org/10.1029/2018GL079195

Li, Y., Kalnay, E., Motesharrei, S., Rivas, J., Kucharski, F., Kirk-Davidoff, D., et al. (2018). Climate model shows large-scale wind and solar farms in the Sahara increase rain and vegetation. *Science*, *361*(6406), 1019–1022.

IPCC. (2018). Global warming of 1.5°C. In V. Masson-Delmotte, P. Zhai, H. O. Pörtner, D. Roberts, J. Skea, P. R. Shukla, et al. (Eds.), *An IPCC Special Report on the impacts of global warming of 1.5°C above pre-industrial levels and related global greenhouse gas emission pathways, in the context of strengthening the global response to the threat of climate change, sustainable development, and efforts to eradicate poverty*. Geneva, Switzerland: World Meteorological Organization.

Muschitiello, F., Zhang, Q., Sundqvist, H. S., Davies, F. J., & Renssen, H. (2015). Arctic climate response to the termination of the African humid period. *Quaternary Science Reviews*, *125*, 91–97.

Parsons, L. A., Brennan, M. K., Wills, R. C. J., & Proistosescu, C. (2020). Magnitudes and spatial patterns of interdecadal temperature variability in CMIP6. *Geophysical Research Letters*, *47*, e2019GL086588. https://doi.org/10.1029/2019GL086588

Pausata, F. S., Emanuel, K. A., Chiacchio, M., Diro, G. T., Zhang, Q., Sushama, L., et al. (2017a). Tropical cyclone activity enhanced by Sahara greening and reduced dust emissions during the African Humid Period. *Proceedings of the National Academy of Sciences*, *114*(24), 6221–6226.

Pausata, F. S., Messori, G., & Zhang, Q. (2016). Impacts of dust reduction on the northward expansion of the African monsoon during the Green Sahara period. *Earth and Planetary Science Letters*, *434*, 298–307.

Purves, D., & Pacala, S. (2008). Predictive models of forest dynamics. *Science*, *320*(5882), 1452–1453.

Raj, J., Bangalath, H. K., & Stenchikov, G. (2019). West African monsoon: Current state and future projections in a high-resolution AGCM. *Climate Dynamics*, *52*, 6441–6461.

Shafiee, S., & Topal, E. (2009). When will fossil fuel reserves be diminished? *Energy Policy*, *37*(1), 181–189.

Sieminski, A. (2013). *International energy outlook 2013 (Report Number: DOE/EIA-0484)*, Washington, DC: US Energy Information Administration (EIA).

Smith, B., Prentice, I. C., & Sykes, M. T. (2001). Representation of vegetation dynamics in the modelling of terrestrial ecosystems: Comparing two contrasting approaches within European climate space. *Global Ecology and Biogeography*, *10*(6), 621–637.

Smith, B., Warlind, D., Arneth, A., Hickler, T., Leadley, P., Siltberg, J., &(2014). Implications of incorporating N cycling and N limitations on primary production in an individual-based dynamic vegetation model. *Biogeosciences*, *11*, 2027–2054.

Sylla, M., Gaye, A., Jenkins, G., Pal, J. S., & Giorgi, F. (2010). Consistency of projected drought over the Sahel with changes in the monsoon circulation and extremes in a regional climate model projections. *Journal of Geophysical Research*, *115*, D16108. https://doi.org/10.1029/2009JD012983

Van Hengstum, P. J., Donnelly, J. P., Fall, P. L., Toomey, M. R., Albury, N. A., & Kakuk, B. (2016). The intertropical convergence zone modulates intense hurricane strikes on the western North Atlantic margin. *Scientific Reports*, *6*, 21728.

Verhoef, A., & Vidale, P. L. (2012). The role of skin layer heat transfer in the surface energy balance. In *Workshop on Workshop on Diurnal cycles and the stable boundary layer*, 7–10 November 2011, ECMWF, ECMWF, Shinfield Park, Reading, pp. 223–233.

Whitley, R., Beringer, J., Hutley, L. B., Abramowitz, G., De Kauwe, M. G., Evans, B., et al. (2017). Challenges and opportunities in land surface modelling of savanna ecosystems. *Biogeosciences*, *14*, 4711–4732.

Wolf, A., Ciais, P., Bellassen, V., Delbart, N., Field, C. B., & Berry, J. A. (2011). Forest biomass allometry in global land surface models. *Global Biogeochemical Cycles*, *25*, GB3015. https://doi.org/10.1029/2010GB003917

Xue, Y., De Sales, F., Lau, W.-M., Boone, A., Feng, J., Dirmeyer, P., et al. (2010). Intercomparison and analyses of the climatology of the west African monsoon in the west African monsoon modeling and evaluation project (WAMME) first model intercomparison experiment. *Climate Dynamics*, *35*(1), 3–27.

Yu, H., Chin, M., Yuan, T., Bian, H., Remer, L. A., Prospero, J. M., et al. (2015). The fertilizing role of African dust in the Amazon rainforest: A first multiyear assessment based on data from cloud-aerosol Lidar and infrared pathfinder satellite observations. *Geophysical Research Letters*, *42*, 1984–1991. https://doi.org/10.1002/2015GL063040

Zhang, X., & Xu, M. (2020). Assessing the effects of photovoltaic powerplants on surface temperature using remote sensing techniques. *Remote Sensing*, *12*(11), 1825.

Zheng, X., & Eltahir, E. A. (1998). The role of vegetation in the dynamics of West African monsoons. *Journal of Climate*, *11*(8), 2078–2096.

References From the Supporting Information

Camargo, S. J., Emanuel, K. A., & Sobel, A. H. (2007). Use of a genesis potential index to diagnose ENSO effects on tropical cyclone genesis. *Journal of Climate*, *20*(19), 4819–4834.

Claussen, M., Kubatzki, C., Brovkin, V., Ganopolski, A., Hoelzmann, P., & Pachur, H. J. (1999). Simulation of an abrupt change in Saharan vegetation in the mid-Holocene. *Geophysical Research Letters*, *26*(14), 2037–2040.

Fathi, M., Abderrezek, M., & Grana, P. (2017). Technical and economic assessment of cleaning protocol for photovoltaic power plants: Case of Algerian Sahara sites. *Solar Energy*, *147*, 358–367.

Green, M. A., Dunlop, E. D., Levi, D. H., Hohl-Ebinger, J., Yoshita, M., & Ho-Baillie, A. W. Y. (2019). Solar cell efficiency tables (version 54). *Progress in Photovoltaics: Research and Applications*, *27*(7), 565–575. https://doi.org/10.1002/pip.3171

Hély, C., & Lézine, A.-M. (2014). Holocene changes in African vegetation: Tradeoff between climate and water availability. *Climate of the Past*, *10*(2), 681–686. https://doi.org/10.5194/cp-10-681-2014

Keenlyside, N. S., & Latif, M. (2007). Understanding equatorial Atlantic interannual variability. *Journal of Climate*, *20*(1), 131–142.

Kutzbach, J. E., & Liu, Z. (1997). Response of the African monsoon to orbital forcing and ocean feedbacks in the middle Holocene. *Science*, *278*(5337), 440–443.

Larrasoaña, J. C., Roberts, A. P., & Rohling, E. J. (2013). Dynamics of green Sahara periods and their role in hominid evolution. *PLoS One*, *8*(10), e76514.

Lavender, S. L., Walsh, K. J. E., Caron, L.-P., King, M., Monkiewicz, S., Guishard, M., et al. (2018). Estimation of the maximum annual number of North Atlantic tropical cyclones using climate models. *Science Advances*, *4*(8). eaat6509.

Neelin, J. D., Jin, F.-F., & Syu, H.-H. (2000). Variations in ENSO phase locking. *Journal of Climate*, *13*(14), 2570–2590.

Pausata, F. S., Zhang, Q., Muschitiello, F., Lu, Z., Chafik, L., Niedermeyer, E. M., et al. (2017b). Greening of the Sahara suppressed ENSO activity during the mid-Holocene. *Nature Communications*, *8*, 16020. https://doi.org/10.1038/ncomms16020

Philander, S. G. (1990). In: El Niño, La Niña, and the Southern Oscillation (Vol. 46). London: Academic Press.

Santbergen, R., & van Zolingen, R. J. C. (2008). The absorption factor of crystalline silicon PV cells: A numerical and experimental study. *Solar Energy Materials and Solar Cells*, *92*(4), 432–444.

Swann, A. L. S., Fung, I. Y., Liu, Y., & Chiang, J. C. H. (2014). Remote vegetation feedbacks and the mid-Holocene green Sahara. *Journal of Climate*, *27*(13), 4857–4870.

Tierney, J. E., Pausata, F. S. R., & deMenocal, P. B. (2017). Rainfall regimes of the green Sahara. *Science Advances*, *3*(1), e1601503.

Trenberth, K. E., & Caron, J. M. (2001). Estimates of meridional atmosphere and ocean heat transports. *Journal of Climate*, *14*(16), 3433–3443.

Xie, S.-P., & Carton, J. A. (2004). Tropical Atlantic variability: Patterns, mechanisms, and impacts. *Earth climate: The ocean–atmosphere interaction. Geophysical Monograph Series*, *147*, 121–142.